Density Functional Theory Study of the β-Carotene Radical Cation

Fahmi Himo*

Department of Molecular Biology, 10550 North Torrey Pines Road, TPC-15, The Scripps Research Institute, La Jolla, California 92037

Received: April 18, 2001; In Final Form: June 12, 2001

The hybrid density functional theory method B3LYP is employed to study the β-carotene radical cation. The radical is characterized by means of its geometry, spin distribution, and isotropic and anisotropic hyperfine coupling constants. It is shown that the spin is delocalized over the whole π-conjugated system, including the double bonds of the headgroups. This delocalization results in methyl hyperfine coupling constants lower than 9 MHz, in excellent agreement with recent experimental couplings of the carotene radical in Photosystem II and in vitro, but in conflict with previous theoretical calculations. It is also demonstrated that rotation of the headgroups can affect the properties of the radical, in particular the spin delocalization to the ring.

I. Introduction

The carotene radical cation has been detected in Photosystem II (PSII) reaction center for quite some time now.[1−6] The carotene cofactor can act as an alternate electron donor under conditions where the primary electron donor pathway is inhibited. The radical has received renewed interest recently.[7−12] Hanley et al. showed that illumination of Mn-depleted PSII at low temperature (20 K) generates the β-carotene radical cation in near stoichiometric quantities.[7] By elevating the temperature to 120−200 K, the carotene radical is reduced and a chlorophyll radical appears. At low field, the electron paramagnetic resonance (EPR) signals from these two radicals are indistinguishable, with a broad unresolved line shape of ca. 10 G and an average *g*-value close to the free electron value.

Brudvig and co-workers have studied this process and characterized the two radicals using a variety of techniques, such as infrared (IR), FT-Raman, and EPR spectroscopies.[10,11]

Faller et al. used pulsed electron nuclear double resonance (ENDOR) spectroscopy to distinguish the two radicals and characterize them.[12] Carotene radicals in PSII and organic solvent gave very similar spectra, showing couplings from six methyl groups (three distinct positions), with the largest methyl coupling in the order of 8−9 MHz in both cases. These results suggested the spin to be delocalized over the molecule.

Earlier EPR experiments from the Kispert lab, where carotenoid radicals have been studied extensively, gave somewhat different results.[13−15] The experiments were done on Nafion film, silica gel, and silica−alumina solid supports, and showed the largest methyl hyperfine couplings on the order of 13−16 MHz. On the basis of semiempirical INDO-type calculations, these large couplings were assigned to the 13,13′ positions (see Figure 1 for numbering), indicating high spin concentration at the middle of the polyene chain.

To address this ambiguity and further characterize the carotene radical cation, we have in the present work performed density functional calculation using the hybrid functional B3LYP.[16] To our knowledge, the only quantum chemical calculations on this system are those by Kispert and co-workers.[13] These are INDO and RHF-INDO/SP calculations based on AM1 geometries.

Despite the size of the system (close to 100 atoms), it is today possible to use more accurate methods. Density functional theory has been extensively tested and employed for this kind of applications, and has been proven to yield hfc's generally in excellent agreement with experiments.[17]

II. Computational Details

The calculations reported in the present study were carried out using the density functional theory (DFT) functional B3LYP,[16] as implemented in the *Gaussian98* program package.[18] The geometry was optimized with the double-ζ plus polarization basis set 6-31G(d,p), with no symmetry constraints. The number of basis functions is 880, constituted of 1512 primitive Gaussians. The spin densities reported are calculated using standard Mulliken population analysis.

For future studies it is useful to note that optimization at the much cheaper B3LYP/3-21G level (472 basis functions, 768 primitive Gaussians) gives very similar geometries to those obtained at the B3LYP/6-31G(d,p) level. Furthermore, single point calculations on the B3LYP/3-21G geometries with the 6-31G(d,p) basis set yield very similar spin populations and hyperfine coupling constants to those obtained when optimizing at the B3LYP/6-31G(d,p) level.

III. Results and Discussion

a. Geometry. The all-trans β-carotene radical cation was found to have two distinct isoenergetic minima. The geometries of these differ in the orientation of the cyclohexene ring relative the polyene chain. One minimum is found with ∠C5−C6−C7−C8 and ∠C5′−C6′−C7′−C8′ dihedral angles of 170.6° (structure I in Figure 1) and the other with dihedral angles of 34.3° (structure II in Figure 1). At the B3LYP/6-31G(d,p) level of theory, structure I has negligible 0.2 kcal/mol lower energy than structure II. Hessian calculations at the B3LYP/3-21G level confirmed that these two minima are true ones, with no imaginary frequencies. Selected geometrical parameters for the two structures are listed in Table 1.

Apart from numerical deviations, both structures adopted *C*2 symmetry, although no symmetry constraints were imposed in the geometry optimization procedure.

* Fax: 1-858-784-8896. E-mail: fhimo@scripps.edu.

10.1021/jp011473a CCC: $20.00
Published on Web 07/24/2001

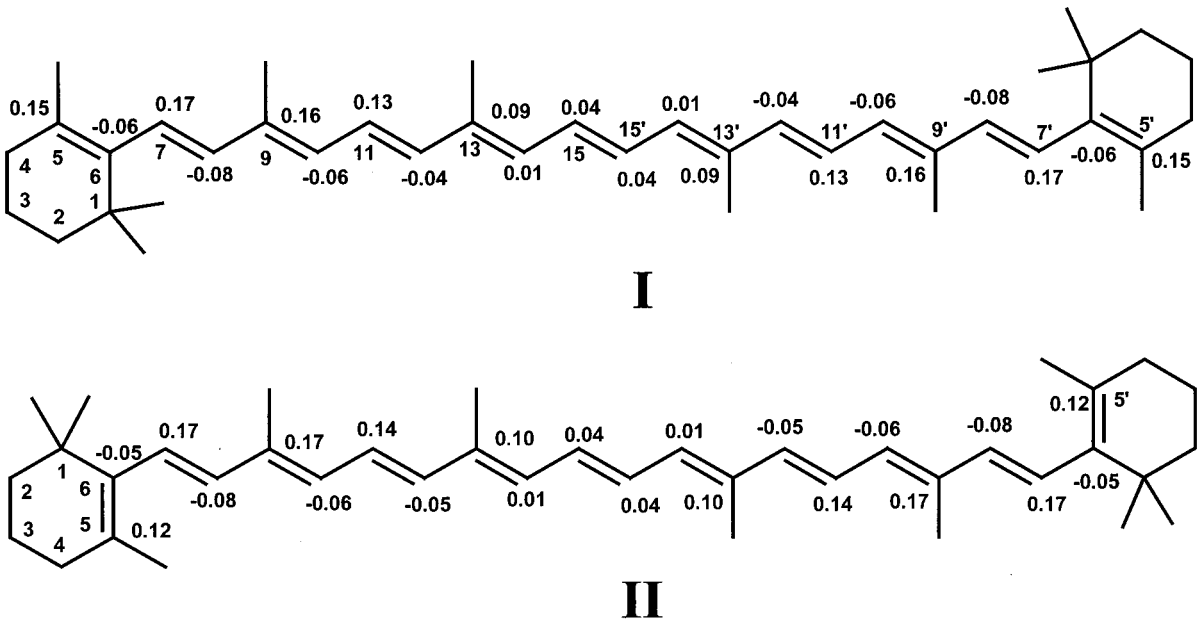

Figure 1. Numbering scheme and B3LYP/6-31G(d,p) calculated spin density distributions of the two isoenergetic minima optimized for the β-carotene radical cation.

TABLE 1: Selected Geometrical Parameters [angstrom and degrees] for the Two Minima Obtained with B3LYP/6-31G(d,p) for Carotene Radical Cation

	structure I	structure II
C1−C2	1.551	1.547
C2−C3	1.524	1.526
C3−C4	1.525	1.526
C4−C5	1.508	1.511
C5−C6	1.378	1.369
C6−C1	1.549	1.552
C6−C7	1.448	1.455
C7−C8	1.374	1.370
C8−C9	1.430	1.433
C9−C10	1.394	1.392
C10−C11	1.405	1.406
C11−C12	1.391	1.390
C12−C13	1.409	1.410
C13−C14	1.407	1.407
C14−C15	1.393	1.394
C15−C15′	1.399	1.399
∠C5−C6−C7	117.0	123.0
∠C5−C6−C7−C8	170.6	34.3

In structure I, the two methyl groups at position 1 lie on opposite sides of the π-plane, minimizing the repulsion to the H8 proton and maintaining therefore a close-to-planar geometry. In structure II on the other hand, the repulsion between the H8 proton and the methyl group at position 5 causes the headgroups to rotate out of the polyene plane with a ∠C5−C6−C7−C8 dihedral angle of 34.3. The ∠C5−C6−C7 angle is then widened to 123° compared to 117° in the case of structure I.

From Table 1 we note that the two structures have very similar bond lengths. The molecule is strongly conjugated, with the difference between single and double bonds being smaller at the middle of the polyene chain than toward the sides. For example, the difference between the central C14−C15 and C15−C15′ bonds in structure I is 0.006 Å (1.393 vs 1.399 Å), while closer to the headgroups, the difference between the C6−C7 and C7−C8 bonds is 0.074 Å (1.448 vs 1.374 Å).

b. Spin Distribution. The relatively low ENDOR methyl hyperfine couplings (<9 MHz) observed by Faller et al.[12] suggest the unpaired spin to be quite delocalized over the conjugated system. Indeed, the B3LYP calculations show that this is the case. The calculated spin densities for structures I and II are displayed in Figure 1. Overall the two minima show very similar spin distributions. The molecule exhibits an odd-alternant spin pattern, with positive spins alternating with smaller negative spins. The largest spins on the polyene chain are found at positions 7,7′ (0.17), 9,9′ (0.16), 11,11′ (0.13), and 13,13′ (0.09).

An interesting result here is that there is significant spin delocalization onto the double bonds of the ring headgroups. Due to the larger rotation of the headgroup (and hence smaller degree of conjugation) in II compared to I, the spin delocalization to the cyclohexene ring is smaller in the former than the latter. The C5 and C6 centers carry respectively 0.15 and −0.06 of the unpaired spin in structure I, compared to 0.12 and −0.05 in structure II.

c. Hyperfine Coupling Constants. The ^{1}H-hyperfine couplings of β-carotene can be divided in two classes: methyl proton couplings and α-proton couplings. In frozen solution, methyl protons give rise to intense and narrow ENDOR lines, while α-protons give rise to broadened lines, which normally escape detection.

The B3LYP/6-31G(d,p) calculated methyl hyperfine couplings are given in Table 2, together with available experimental couplings and previous INDO and RHF−INDO/SP theoretical results. β-carotene has six methyl groups in three distinct positions (5, 9, and 13). We expect the magnitude of the hyperfine couplings of these to be such that $A_{iso}(9) > A_{iso}(5) > A_{iso}(13)$, since the spin densities at these positions show this trend.

The largest calculated isotropic coupling was indeed found on the 9,9′ positions. The magnitude was ca. 8 MHz, in good agreement with the largest coupling detected in PSII (7.2 MHz) and the model system (7.3 MHz) by Faller et al.[12] In the solid support experiments by Kispert and co-workers,[14,15] the largest coupling was found to be >13 MHz, and was assigned to the 13,13′ positions based on the INDO and RHF-INDO/SP calculations (ca. 16 and 12 MHz, respectively). A methyl coupling of this magnitude is lacking in our B3LYP calculations. The calculations predict the 13,13′ positions to have the smallest methyl couplings (ca. 5 MHz), in reasonably good agreement

TABLE 2: Hyperfine Coupling Constants [MHz] for Methyl Protons in β-Carotene Radical Cation

molecular position		B3LYP/6-31G(d,p)[a] I	B3LYP/6-31G(d,p)[a] II	PSII[b]	in vitro[b]	in vitro[c]	in vitro[d]	INDO[e]	RHF-INDO/SP[e]
5,5′	A_{11}	8.4	7.8	3.3	2.5	2.5	1.9		
	A_{22}	6.8	6.5	3.3	3.7	2.5	1.9		
	A_{33}	6.4	6.1	3.3	2.5	2.8	2.0		
	A_{iso}	7.2	6.8	3.3	2.9	2.6	1.9	5.9/6.4	2.2/2.3
9.9′	A_{11}	9.2	9.7	7.2	6.5	8.8	8.2		
	A_{22}	8.0	8.3	7.2	8.5	8.8	8.2		
	A_{33}	7.1	7.5	7.2	7.0	9.2	8.5		
	A_{iso}	8.1	8.5	7.2	7.3	8.9	8.3	16.0	8.1/8.5
13,13′	A_{11}	5.6	5.9	5.5	2.6	15.9/12.8	13.0		
	A_{22}	4.7	5.1	5.0	3.8	15.9/12.8	13.0		
	A_{33}	4.1	4.3	4.5	2.6	17.0/14.2	13.0		
	A_{iso}	4.8	5.1	5.0	3.0	16.2/13.3	13.0	16.2	12.2/12.5

[a] This work, methyl hyperfine coupling constants are calculated as an average of the couplings of the three methyl protons, [b] Ref 12. [c] Ref 14. [d] Ref 15. [e] Ref 13.

TABLE 3: B3LYP/6-31G(d,p) Calculated ^{1}H Hyperfine Coupling Constants [MHz] for Carotene Radical Cation

molecular position	A_{11}	A_{22}	A_{33}	A_{iso}
		Structure I		
4,4′	21.5	19.6	19.1	20.0
	12.4	10.2	10.0	10.9
7,7′	−14.6	−11.1	−5.7	−10.4
8,8′	6.2	3.0	2.6	3.9
10,10′	4.5	1.7	1.4	2.5
11,11′	−12.0	−9.0	−4.2	−8.4
12,12′	4.1	1.2	1.0	2.1
14,14′	−2.2	−2.1	0.6	−1.2
15,15′	−3.4	−3.2	−2.2	−2.9
		Structure II		
4,4′	14.7	13.0	12.6	13.5
	11.6	10.1	9.8	10.5
7,7′	−16.7	−12.0	−6.0	−11.6
8,8′	6.5	2.8	2.4	3.9
10,10′	4.7	1.9	1.5	2.7
11,11′	−12.7	−9.6	−4.4	−8.9
12,12′	4.3	1.3	1.0	2.2
14,14′	−2.2	−2.2	0.5	−1.3
15,15′	−4.5	−3.9	−0.9	−3.1

with the smallest coupling in PSII (3.3 MHz), which was assigned to the 5,5′ positions.[12] Our calculated couplings for the 5,5′ positions are ca. 7 MHz and compare fairly well with the measured intermediate coupling (5.0 MHz in PSII).

The spin at C5 induces hyperfine couplings at the H4 protons also. These couplings are sensitive to the amount of spin at C5. In structure I, where the C5 spin is 0.15, the isotropic H4 couplings are 20.0 and 10.9 MHz, whereas in structure II (C5 spin = 0.12) they are 13.5 and 10.5 MHz.

The largest isotropic polyene chain α-proton hfc's are found at 7,7′ and 11,11′ positions (∼11 and 8 MHz), reflecting the high spin population at these centers (0.17 and 0.14, respectively). The other α-protons have much smaller hfc's, lower than 4 MHz (see Table 3).

Table 3 also shows that the H4 couplings and the methyl proton coupling show little anisotropy, while the α-proton couplings are highly anisotropic.

d. Rotation of Headgroups. Structures I and II have very similar overall geometric, spin, and hyperfine properties. However, there are some differences that are related to their different headgroup rotational angles, like for instance the spin on C5 and resulting hyperfine coupling on the methyl group and the H4 protons. We decided therefore to investigate the effects of this rotation on the properties of the carotene radical.

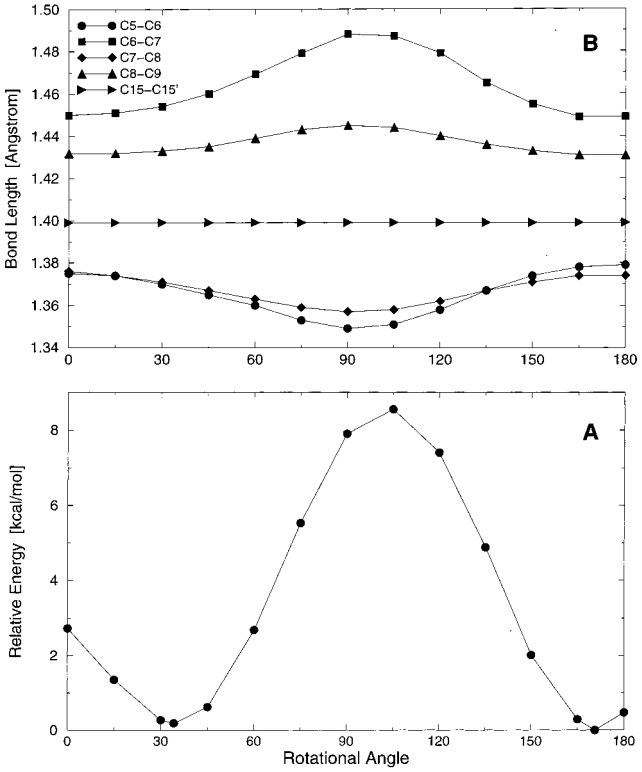

Figure 2. Potential energy curve for rotation around the C6−C7 and C6′−C7′ bonds (A), and the effects of this rotation on selected bond distances (B).

In particular, we wanted to examine if the large methyl coupling observed by Kispert and co-workers can be a result of the headgroup orientation.

The rotation was performed by simultaneously rotating about the C6−C7 and C6′−C7′ bonds, keeping the ∠C5−C6−C7−C8 and ∠C5′−C6′−C7′−C8′ dihedral angles frozen at angles from 0° to 180° in steps of 15°, and optimizing all other degrees of freedom.

In Figure 2 we show the B3LYP/6-31G(d,p) computed potential energy surface associated with this rotation, and the effect of the rotation on selected bond lengths.

The rotational transition state (TS) was optimized and the energy barrier between the two minima (structures I and II) was found to be 8.4 kcal/mol. The TS occurs at 108.2° dihedral angle, where the conjugation is completely broken. It should be noted that the 8.4 kcal/mol barrier is to break the conjugation

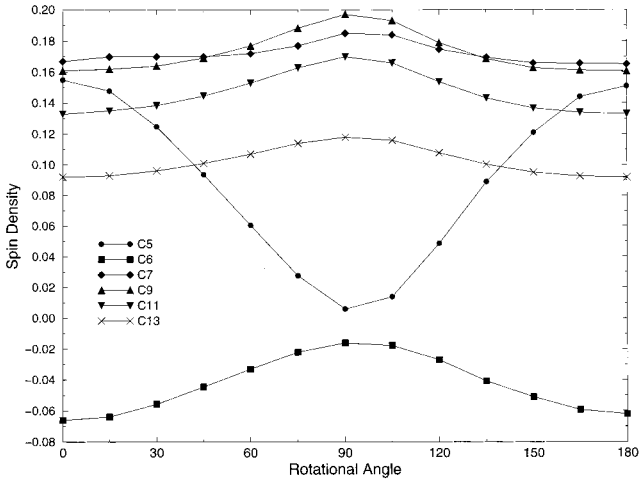

Figure 3. Effects of headgroup rotation on spin density distribution in β-carotene radical cation.

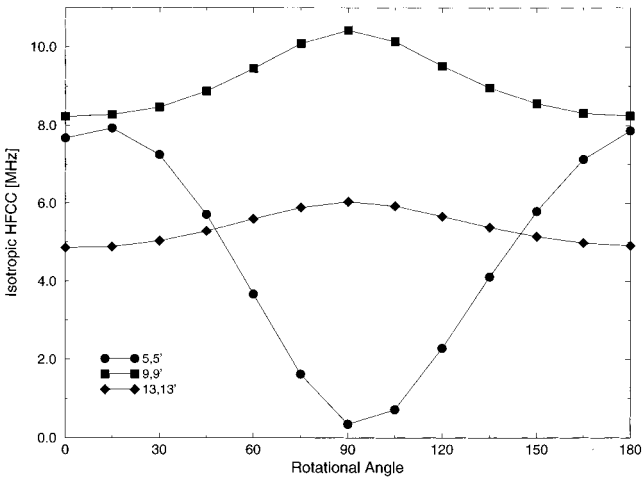

Figure 4. Effects of headgroup rotation on methyl proton hyperfine coupling constants.

of both headgroups, i.e., the barrier is ca. 4 kcal/mol for the rotation of each headgroup.

The bonds affected most by the rotation are the ones closest to the headgroups. As the dihedral angle increases and the conjugation degree decreases, the C5−C6 double bond is shortened (1.375 Å at 0° and 1.349 Å at 90°) and the C6−C7 single bond is elongated (1.450 Å at 0° and 1.488 Å at 90°). The changes in the other bond lengths show a similar pattern, i.e., double bonds become shorter at 90° and single bonds become longer. However, the changes are smaller than for the C5−C6 and C6−C7 bonds, and are diminished toward the middle of the chain. The C15−C15′ bond length, for example, is completely unaffected by the rotation.

The effect of headgroup rotation on the spin distribution is displayed in Figure 3. As expected, maximum delocalization of spin to the ring system is seen for the perfectly planar structures (dihedral angles 0° and 180°). The C5 and C6 centers possess then, respectively, 0.16 and −0.07 of the unpaired spin. These spins vary sinusoidally with the rotational angle, reaching zero at 90°. The spin from C5 and C6 is then redistributed over the other centers. The main changes occur on the C7, C9, C11, and C13 centers, as shown in Figure 3. The spin on C9 increases from 0.16 to 0.20 in going from 0° to 90°. The C11 spin increases with equal amount, from 0.13 to 0.17, while the increase on C13 is 0.03 (from 0.09 to 0.12). The rest of the

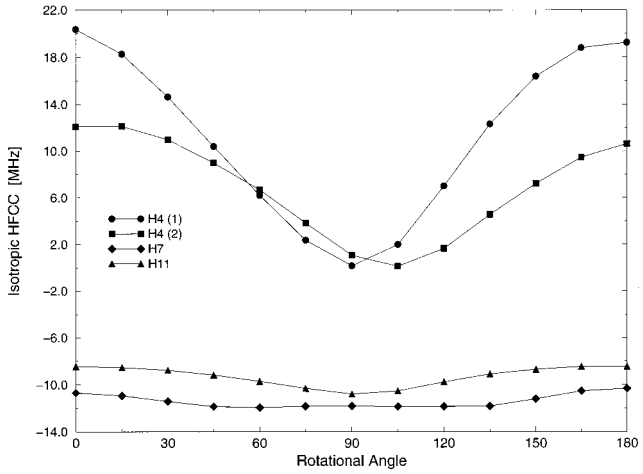

Figure 5. Effects of headgroup rotation on proton hyperfine coupling constants.

centers, in particular those harboring negative spins, change insignificantly.

The strong angle-dependence of the C5-spin induces a similar dependence in the methyl hyperfine couplings at that position (Figure 4). The isotropic methyl hfc decreases from 8 to 0 MHz in going from 0° to 90°, and increases back to 8 MHz when the conjugation is restored at 180°, correlating perfectly with the C5 spin. Also the methyl couplings at positions 9 and 13 correlate with their spins; maximum values for these couplings are reached at 90°, 10.4 and 6.0 MHz, respectively.

Clearly, none of them reaches up to the 13 MHz coupling observed in solid support experiments. Given the good agreement between our ground-state hyperfine couplings and the solution and PSII ones, one might speculate that somehow the interaction between the carotene radical and the solid support causes spin concentration that results in the large methyl hyperfine coupling.

The H4 proton hyperfine couplings are also greatly affected by the rotation, as a result of the variation of the spin on C5 (Figure 5). In the planar conformations, 0° and 180°, the two protons have isotropic couplings of ca. 20 and 12 MHz. As the spin on C5 drops to zero at perpendicular angles, these couplings vanish.

The polyene chain α-proton coupling change very little due to rotation. The H7 and H11, for instance, change less than 2 MHz (Figure 5).

IV. Conclusions

We have in the present study characterized the β-carotene radical cation by means of its geometry, spin density distribution, and isotropic and anisotropic hyperfine couplings, using density functional theory. The DFT calculations here give a quite different picture of the carotene radical cation from that reported previously. The spin is shown to be delocalized to a much higher extent, resulting in relatively low methyl hyperfine couplings, the highest in the order of 8 MHz. We have demonstrated that rotation of headgroups can modulate the spin and hyperfine properties, in particular the spin delocalization to the cyclohexene ring system and the resulting hyperfine coupling constants there.

Acknowledgment. I thank Dr Fraser MacMillan for suggesting the calculations, and the Wenner-Gren Foundations for financial support.

References and Notes

(1) Dawe, E. A.; Land, E. J. *J. Chem. Soc., Faraday Trans.* **1975**, *71*, 2162.
(2) Velthuys, B. R. *FEBS Lett*. **1981**, *126*, 272.
(3) Schenck, C. C.; Diner, D.; Mathis, P.; Satoh, K. *Biochim. Biophys. Acta* **1982**, *689*, 216.
(4) Mathis, P.; Rutherford, A. W. *Biochim. Biophys. Acta* **1984**, *767*, 217.
(5) Telfer, A.; De La Rivas, J.; Barber, J. *Biochim. Biophys. Acta* **1991**, *1060*, 106.
(6) Noguchi, T.; Mitsuka, T.; Inoue, Y. *FEBS Lett*. **1994**, *356*, 179.
(7) Hanley, J.; Deligiannakis, Y.; Pascal, A.; Faller, P.; Rutherford, A. W. *Biochemsitry* **1999**, *38*, 8189.
(8) Deligiannakis, Y.; Hanley, J.; Rutherford, A. W. *J. Am. Chem. Soc.* **2000**, *122*, 400.
(9) Faller, P.; Rutherford, A. W.; Un, S. *J. Phys. Chem. B* **2000**, *104*, 10960.
(10) Vrettos, J. S.; Stewart, D. H.; de Paula, J. C.; Brudvig, G. W. *J. Phys. Chem. B* **1999**, *103*, 6403.
(11) Tracewell, C. A.; Cua, A.; Stewart, D. H.; Bocian, D. F.; Brudvig, G. W. *Biochemistry* **2001**, *40*, 193.
(12) Faller, P.; Maly, T.; Rutherford, A. W.; MacMillan, F. *Biochemistry* **2001**, *40*, 320.
(13) Piekara-Sady, L.; Khaled, M. M.; Bradford, E.; Kispert, L. D.; Plato, M. *Chem. Phys. Lett.* **1991**, *186*, 143.
(14) Wu, Y.; Piekara-Sady, L.; Kispert, L. D. *Chem. Phys. Lett.* **1991**, *180*, 573.
(15) Jeevarajan, A. S.; Kispert, L. D.; Piekara-Sady, L. *Chem. Phys. Lett.* **1993**, *209*, 269.
(16) (a) Becke, A. D. *Phys. Rev.* **1988**, *A38*, 3098, (b) Becke, A. D. *J. Chem. Phys.* **1993**, *98*, 1372. (c) Becke, A. D. *J. Chem. Phys.* **1993**, *98*, 5648.
(17) See for instance the work of O'Malley, P. J.; Eriksson, L. A.; Barone, V.; Wheeler, R.; and others.
(18) Frisch, M. J.; Trucks, G. W.; Schlegel, H. B.; Scuseria, G. E.; Robb, M. A.; Cheeseman, J. R.; Zakrzewski, V. G.; Montgomery, J. A., Jr.; Stratmann, R. E.; Burant, J. C.; Dapprich, S.; Millam, J. M.; Daniels, A. D.; Kudin, K. N.; Strain, M. C.; Farkas, O.; Tomasi, J.; Barone, V.; Cossi, M.; Cammi, R.; Mennucci, B.; Pomelli, C.; Adamo, C.; Clifford, S.; Ochterski, J.; Petersson, G. A.; Ayala, P. Y.; Cui, Q.; Morokuma, K.; Malick, D. K.; Rabuck, A. D.; Raghavachari, K.; Foresman, J. B.; Cioslowski, J.; Ortiz, J. V.; Baboul, A. G.; Stefanov, B. B.; Liu, G.; Liashenko, A.; Piskorz, P.; Komaromi, I.; Gomperts, R.; Martin, R. L.; Fox, D. J.; Keith, T.; Al-Laham, M. A.; Peng, C. Y.; Nanayakkara, A.; Challacombe, M.; Gill, P. M. W.; Johnson, B.; Chen, W.; Wong, M. W.; Andres, J. L.; Gonzalez, C.; Head-Gordon, M.; Replogle, E. S.; Pople, J. A. *Gaussian98, Revision A.9*; Gaussian, Inc.: Pittsburgh, PA, 1998.